



The effect of applied compressive stress on the diffusion of carbon in carbon supersaturated S-phase layer



Wei Li^{a,*}, Wei Guo^a, Xu Zhu^a, Xuejun Jin^{b,*}, Xiaoying Li^c, Hanshan Dong^c

^a School of Materials Science and Engineering, Shanghai Jiao Tong University, Shanghai 200240, China

^b Collaborative Innovation Center for Advanced Ship and Deep-Sea Exploration, Shanghai Jiao Tong University, Shanghai 200240, China

^c School of Metallurgy and Materials, The University of Birmingham, Birmingham B15 2TT, UK

ARTICLE INFO

Keywords:

Stainless steels

S-phase

Expanded austenite

Hydrostatic compressive stress

Carbon diffusion

ABSTRACT

In this study, hydrostatic compressive stresses are applied on the prior-carburized samples of 316 ASS to discover the relationship between interstitial diffusion process and the applied stresses. Carbon diffusion profiles are compared and concentration dependent diffusion coefficients are discussed to further advance scientific understanding of diffusion process in supersaturated S-phase. The experimental results demonstrate that the applied compressive stress can retard the fast diffusion process comparing to the unstressed one. Based on theoretical modelling, the effect of the applied hydrostatic compressive stresses on the diffusion of carbon in carbon supersaturated 316 austenitic stainless steel is discussed.

1. Introduction

S-phase, interstitial supersaturated expanded austenite, is produced on the surface of austenitic stainless steel by low temperature nitriding, carburizing or carbonitriding. It arouses great interests by performing extremely high hardness, excellent wear resistibility and brilliant fatigue property [1]. It is generally believed that S-phase is an interstitial supersaturated single phase without precipitates [2–4]. Hence, the most significant signature of S-phase, supersaturation, has been verified by many researchers [5–8] and the value of the interstitial supersaturation can reach about 12 at.% in carburized surface S-phase layer and about 25–30 at.% in nitrided ones [9–12].

The earlier prediction of nitrogen depth profiles in plasma nitrided ferrite steel containing nitride forming elements was developed by Sun and Bell et al. [13] and several models have been proposed to explain the tremendous uptake of nitrogen in S-phase. One is the trapping and detrapping model which was developed by Parascandola et al. [14] considering the assumption that diffusion of nitrogen is influenced by trap sites of local chromium. Another model by Mandl et al. [15] assumed that N diffusion in S-phase was concentration dependent, with high diffusion coefficients for high nitrogen contents and low value for low ones. Contrary to the trapping/detrapping model, Mandl et al. [16] studied different steel grades and found that there is no clear correlation between the critical point of nitrogen diffusion and the chromium content. Besides, Abrasonis et al. [17] explained the influence of flux on the ion-beam nitriding of austenitic stainless steel by considering free

diffusion-sputtering. Christiansen et al. [18,19] simulated the diffusion of N in austenitic stainless steel with different equilibrium constants. Recent work by Wu et al. [20] showed that the diffusivity difference between carbon and nitrogen increases with increasing Cr concentration but the carbonitriding results demonstrated that the diffusion depth of carbon or nitrogen is not affected by the presence of each other. Clearly, it is still a challenge to predict the depth distribution of interstitials in S-phase layers despite the great effort made by these researchers.

Meanwhile, an interesting issue kinked with the supersaturation of interstitials in S-phase is the large compressive residual stresses which was evaluated to be about -2.7 GPa for carburized S-phase and even larger for nitrided ones [21,22]. Although thermal stresses may be introduced upon cooling from the treatment temperature to room temperature, the residual stress is mainly induced by the supersaturated interstitials and vice versa the stress conditions can also influence the diffusion of interstitials [23]. Therefore, the diffusion of interstitial atoms in S-phase is complicated by the mutual effects of interstitial compositions and stresses. X-ray diffraction pattern in S-phase showed a shift of the (200) peak comparing with the untreated austenite probably because of stacking faults (SFs) created by cold working [24,25]. Both low temperature carburizing and nitriding show some interesting diffusion phenomenon. Although the effect of the in-situ applied tensile stresses on the formation of S-phase during low-temperature carburizing of 316 steel has been reported in our previous paper [26], to date, no work has been reported on the effect of external compressive stress

* Corresponding authors.

E-mail addresses: weilee@sjtu.edu.cn (W. Li), jin@sjtu.edu.cn (X. Jin).

Table 1
The chemical composition of 316 ASS (at.%).

C	Cr	Ni	Mo	Mn	Si	P	S	Cu	N	Fe
0.23	18.35	10.32	1.18	1.62	0.94	< 0.05	0.01	0.35	0.29	Balance

on carbon supersaturated expanded austenite i.e. S-phase.

In this study, in order to study the effect of external compressive stress on carbon diffusion in carbon supersaturated expanded austenite (i.e. S-phase), hydrostatic compressive stresses are applied through hot isostatic pressing (HIPping) to low-temperature carburised (i.e. carbon S-phase) 316 steel samples. Carbon depth-distribution profiles are carefully measured and compared; carbon diffusion process under the applied compressive stresses is analyzed; and concentration dependent diffusion coefficients are calculated. Finally, the effect of the applied compressive stresses on the diffusion of carbon in the carbon S-phase is discussed to further advance scientific understanding of interstitial diffusion in supersaturated S-phase under compressive stress.

2. Experimental

The material used in this study is 316 austenitic stainless steel with nominal composition shown in Table 1. The samples were cut from hot-rolled bars with diameter of 25 mm into 5.5 mm thick disks, using a high precision Struers Accutom-5 cutting machine, fitted with SiC abrasive cutting blades. Then the samples were wet ground into flat surfaces with SiC grinding paper of grit #120. The one face which was to be carburized was ground further up to grit #1200 (#240, #400, #800 in steps). Then samples were washed in soap water and acetone, both in an ultrasonic bath, for 10 min, then dried with blow-air.

Based on the optimal values identified by previous research [27], low temperature plasma carburizing treatment was carried out in a 60 kW Klöckner DC plasma unit at 500 °C for 10 h in 400 Pa gas mixtures with 1.5% CH₄ and 98.5% H₂. This will also facilitate the comparison with the earlier work on the effect of temperature on the stability of S-phase [23]. After plasma carburizing treatment (sample coded as 'PC'), samples were carefully taken out and swabbed with acetone to remove the superficial very thin deposition layer of amorphous carbon although Fe₃C and oxides were also identified by other researchers [28]. Then samples were separated into two groups and the group one samples were sealed individually in a vacuumed quartz tube with a few refilled argon gas. Then these samples were heated treated heated up to the conditions as listed in Table 1 in a Muffle furnace. For group two, samples were put into an EPSI Lab HIP (Hot Isostatic Pressing) facility and were heated up to designed temperatures with hydrostatic compressive stresses by argon gas for different time as detailed in Table 2. The group one samples were coded as 'HT', and the samples from group two were coded as 'HIP'. Limited by the capacity of the HIP equipment, short soaking time (1–10 h) and relatively high soaking temperature (525–600 °C) were chosen to promote diffusion process while suppress potential carbide precipitations.

Table 2
Sample codes and corresponding HIP and HT treatment conditions for plasma carburized (PC) samples.

Samples code	Temperature °C	Pressure MPa	Soaking time h
HIP/HT 1	525	180/0	10
HIP/HT 2	550	180/0	1
HIP/HT 3	550	180/0	5
HIP 4	575	90	1
HIP/HT 5	575	180/0	1
HIP/HT 6	575	180/0	2
HIP/HT 7	600	180/0	0.5
HIP/HT 8	600	180/0	1

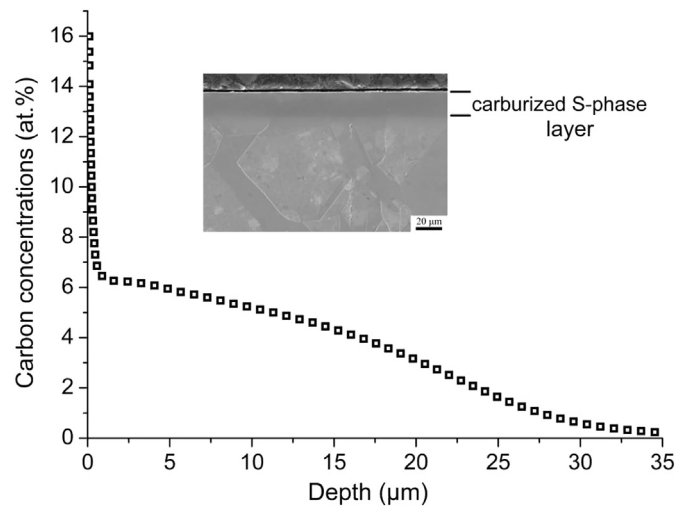


Fig. 1. Carbon depth profile of sample 'PC' prior to HIPping and annealing treatments. Cross sectional SEM image was inserted.

A Leco GDS-750 QDP unit was used to probe the composition-depth profiles of the carburized and tempered samples. In this technique surface atoms were sputtered from the sample and went into the argon plasma, where de-excitation process occurred and each species of particles would emit a characterized spectrum of light from which the quantity of these atoms could be evaluated from the intensity of their specified spectrum. The method and measurement program were calibrated using standard blocks of known composition, according to the instructions of the manufacturer. The measurement was repeated at least three times for each sample and the reproducible results were reported. Cross-sectional microstructures were observed by Jeol 7000 field emission gun (FEG) SEM after grinding and polishing, then etching with a 50% HCl + 25% HNO₃ + 25% H₂O etchant. A Philips X'Pert diffractometer was employed to obtain the x-ray patterns of samples using Cu radiation with K_{α1} 0.15406 nm.

3. Results

A typical carbon profile after carburizing treatment on 316 austenitic stainless steel is illustrated in Fig. 1. It is noteworthy that the highest amount at the top surface can reach above 12 at.%. Then there is a plateau at about 6.5 at.% before it gradually depleted into the substrate.

Fig. 2 shows the carbon depth profiles of samples 'HT 1' and 'HIP 1' comparing with 'PC'. The trend of carbon depth profiles revealed that the maximum carbon content near the surface was significantly reduced but the thickness of the surface case was increased after HIPping and HT treatments due to inward diffusion of carbon during these treatments. However, it can be deduced by comparing the carbon depth profiles in the 'HT 1' and 'HIP 1' samples that the compressive stress applied by HIPping treatment retarded the diffusion of carbon atoms from the carburized surface cases towards the central substrate. Consequently, the 'HIP 1' sample had a high carbon quantity in the top surface case of about 25 μm but a shallow carbon penetration into the substrate.

Similar phenomenon was observed for samples heated up to 550, 575 and 600 °C. This is further supported by the effect of compressive stress levels on the diffusion of carbon at 575 °C for 1 h. As shown in Fig. 3, the carbon depth profile of the 90 MPa HIPped sample ('HIP 4') was located in-between those of the 0 MPa ('HT 5') and 180 MPa ('HIP 5') treated samples. For the same diffusion time (1 h) but at different temperatures, the carbon diffusion profiles behave differently as shown in Fig. 4.

Fig. 5 show the XRD charts of HIP and HT samples treated at a

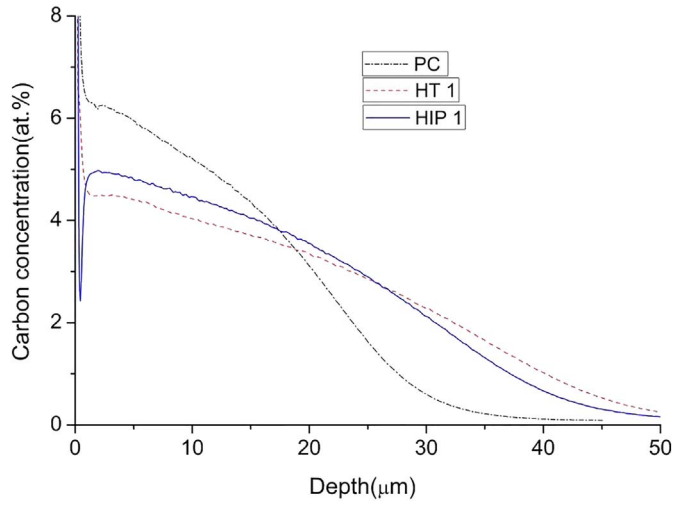


Fig. 2. Carbon depth profiles of Sample 'PC', 'HT 1' (525 °C, 10 h) and 'HIP 1' (525 °C, 180 MPa, 10 h).

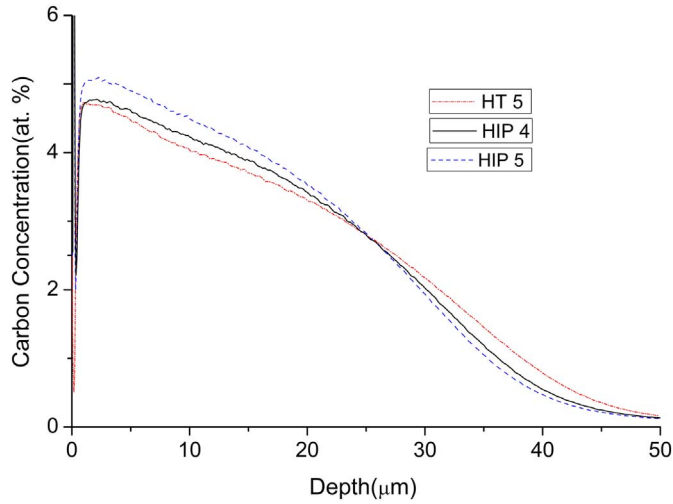


Fig. 3. Carbon depth profiles of Sample 'HT 5' (575 °C, 1 h), 'HIP 4' (575 °C, 180 MPa, 1 h) and 'HIP 5' (575 °C, 90 MPa, 1 h).

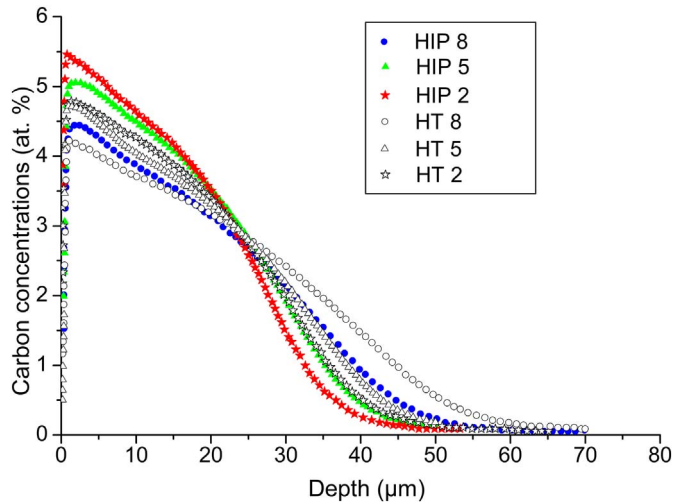


Fig. 4. Carbon profiles of carburized samples after heat treatment at 550 °C, 575 °C and 600 °C for 1 h under 0 (HT) and 180 MPa (HIP) isostatic compressive stress.

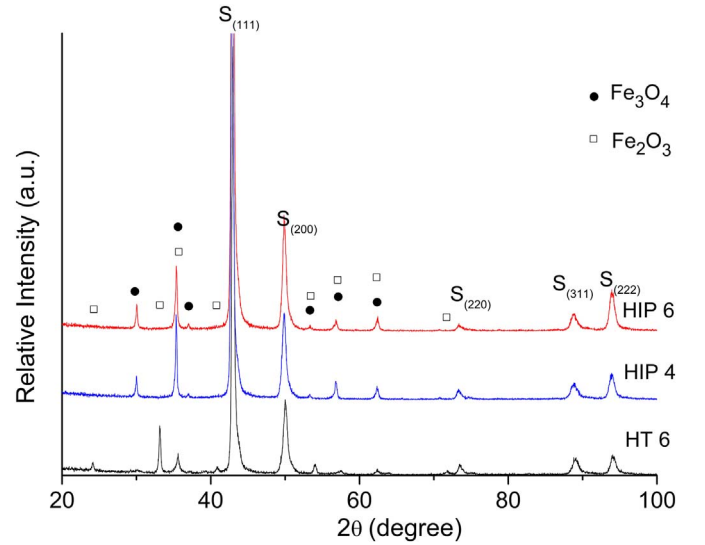


Fig. 5. XRD charts of HIP and HT treated PC samples at 575 °C.

relatively high temperature of 575 °C. Peaks from the S-phase and oxides can be clearly seen but no appreciable precipitates or bcc structured iron could be identified from the XRD charts of the samples. The oxide peaks implies that oxidation occurred to the sample surfaces mainly due to the residual oxygen in the argon gas used for HT and HIP treatment. The thin surface oxide film could act as a barrier to outward diffusion of carbon (i.e. decarburisation) during the HT and HIP processes.

4. Discussion

4.1. Diffusion of carbon interstitials in expanded austenite

The diffusion process with limited source of carbon which is introduced by previous carburizing treatment. The carbon composition depth profiles following heat treatments under compressive hydrostatic stress (HIP) and zero stress (HT) at different temperatures are examined in the composition dependent diffusivity model, the general Fick's second law:

$$\frac{\partial c}{\partial t} = \frac{\partial}{\partial x} \left(D(c) \frac{\partial c}{\partial x} \right) \quad (1)$$

Introducing a scaling variable, $\xi = \frac{x-x_s}{\sqrt{t_s+t}}$ [15,29,30], Eq. (1) is transformed to:

$$-\frac{\xi}{2} \frac{dc}{d\xi} = \frac{d}{d\xi} \left(\tilde{D} \frac{dc}{d\xi} \right) \quad (2)$$

In the case where t is a constant the solution of $D(c)$ can be obtained from Eq. (2):

$$D(c) = \frac{-1}{2(t_s+t)} \left(\frac{dx}{dc} \right) \Big|_{c_0} \cdot \int_{c_0}^c (x-x_s) \cdot dc' \quad (3)$$

where c_0 is the concentration at the inner boundary of the carburizing layer, where $\left(\frac{dc}{dx} \right) \Big|_{c_0} = 0$. Since $c(x)$ is known, therefore $\tilde{D}(c)$ can be obtained by integrating Eq. (3) starting from c_0 . x_s and t_s can be solved by equating the ξ s corresponding to the same compositions of different $c(x)$ curves.

The validity of the transformation of $c(x,t)$ to $c(\xi)$ is shown in Fig. 6.

The $c(\xi)$ curves of $T = 550$ °C under the condition of HT. The blue curve is for the initial condition ($t = 0$ h) and the red curve is for $t = 1$ h. $x_s = 18.29$ and $t_s = 0.35$. The two curves fit with each other fairly well, which validates the transformation of $c(x,t)$ to $c(\xi)$ with

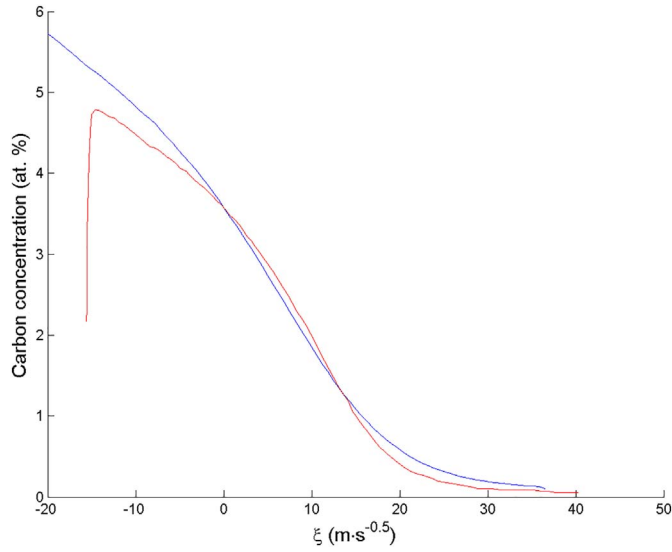


Fig. 6. The concentration profiles after transformation of $c(x, t)$ to $c(\xi)$.

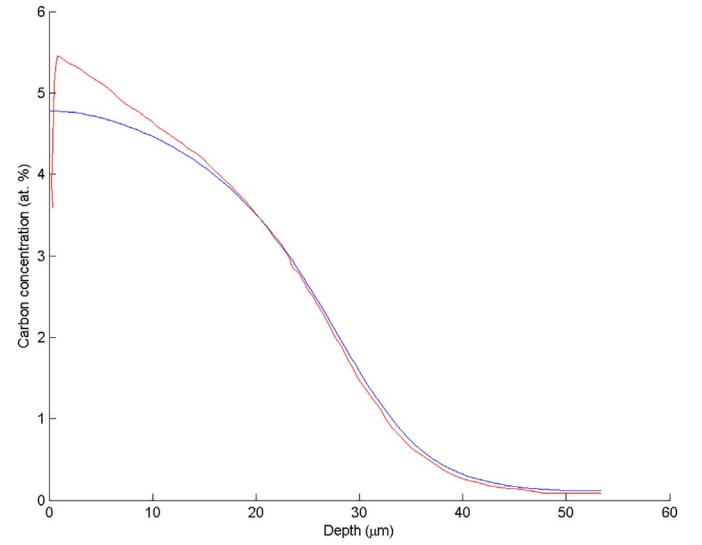


Fig. 8. The comparison between the simulated concentration profile (blue) at $t = 1$ h, $T = 550$ °C under HIP condition and the experimental concentration profile (red) of the same conditions. The simulated concentration profile is obtained using the initial concentration profile ($t = 0$ h) and the calculated diffusivity of $T = 550$ °C under HIP condition. (For interpretation of the references to color in this figure legend, the reader is referred to the web version of this article.)

$$\xi = \frac{x - x_s}{\sqrt{t_s + t}}$$

The calculated carbon diffusion coefficient via carbon concentrations are shown in Fig. 7. It is apparent that carbon diffusion coefficient change with the carbon concentrations and the carbon diffusivity is much higher in HT samples than that in HIP samples.

An attempt has been to validate the model used to calculate the diffusivities in Fig. 7. The evolution of the concentration profile of $T = 550$ °C and HIP condition is simulated using the calculated diffusivity of the same condition, which is denoted as HIP2 in Fig. 7. The simulation is carried out by integrating the diffusion equation (Eq. (1)) using concentration-dependent $D(c)$. The initial condition is the concentration profile of $t = 0$ h. The simulated concentration profile of $t = 1$ h is shown in Fig. 8 and it is compared to the experimental concentration profile of the same conditions. The comparison shows that the experimental concentration profile agrees fairly well with the simulated one. This implies that the calculated diffusivities in Fig. 7 are fairly precise and thus the model, from which these diffusivities are calculated, is validated.

4.2. Effect of self-stress on diffusion in expanded austenite: an elastic analysis

The effect of self-stress on diffusion is an interesting topic, and the original idea can trace back to the earlier research work by Larché and Cahn [31–33]. In the small strain approximation, the stress-strain law can be written as:

$$E_{ij} - E_{ij}^c = s_{ijkl} T_{kl} \quad (4)$$

where, s_{ijkl} is the compliance tensor, E_{ij}^c is the stress free composition strain tensor, T_{kl} is the stress tensor. And the diffusion potential under the effect of stress can be expressed:

$$M(T, c) = M(0, c) - \frac{1}{\rho_0} \left(\frac{dE_{ij}^c}{dc} T_{ij} + \frac{ds_{ijkl}}{dc} T_{ij} T_{kl} \right) \quad (5)$$

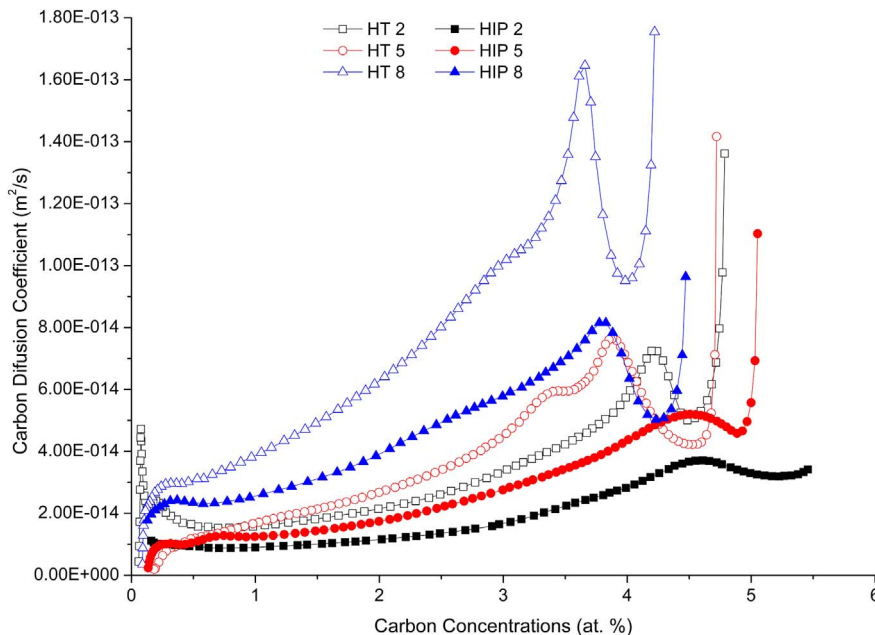


Fig. 7. The calculated carbon diffusion coefficient as a function of the carbon concentrations and temperature for HT and HIP samples (HT/HIP 2 for 550 °C, HT/HIP 5 for 575 °C and HT/HIP 8 for 600 °C).

ρ_0 is molar density of lattice sites, and its inverse V_0 is the molar volume of lattice sites, which is generally referred. Simpler case of diffusion in isotropic solids, it is assumed that $\frac{dE_{ij}^c}{dc} = \eta\delta_{ij}$ is a constant and the variation of elastic coefficients with composition are sufficiently small to be neglected.

$$\text{Where, } \delta_{ij} = \begin{cases} 1, & i = j \\ 0, & i \neq j \end{cases}$$

The half-space geometry renders the diffusion problem to be one dimensional when the z-axis is normal to the surface and pointing towards the solid. For the carbon diffusion of prior-carburized sample, the stress is zero at $z = \infty$, and the stress profile can be evaluated by the residual stress measurement of just carburized sample.

The flux is proportional to the gradient of the diffusion potential

$$J_z = -B \left[\frac{dM(0, c)}{dc} + \frac{2\eta^2 Y}{\rho_0} \right] \frac{dc}{dz} \quad (6)$$

In general B is a function of the local temperature θ , stress T and composition c ; Y is a function which has been derived and used in the theory on stress effect on Spinodal decomposition [34,35], and reduced to be $Y = E/(1 - \nu)$ (E is Young's modulus and ν is Poisson's ratio) when the crystal is isotropic.

By comparing with the Fick's first law, the apparent diffusion coefficient for interstitial solutions is given:

$$D_{app} = B \left[\frac{dM(0, c)}{dc} + \frac{2\eta^2 Y}{\rho_0} \right] \quad (7)$$

When B is independent of stress, the apparent diffusion coefficient (D_{app}) can be expressed by

$$D_{app} = D_{zero} \left[1 + \frac{\partial \ln \gamma}{\partial \ln c} + \frac{2\eta^2 Y c}{\rho_0 RT} \right] \quad (8)$$

where D_{zero} is the general diffusion coefficient with no diffusion induced stress and γ is the activity coefficient, c is the molar concentration of carbon; T is the absolute temperature and R is the gas constant.

In multi-component austenite, the activity coefficient can be expressed by the following equation which is a function of absolute temperature [36]:

$$\begin{aligned} \ln \gamma = & \frac{2300}{T} - 0.92 + \left(\frac{3860 + 10000y_{Si}}{T} \right) y_{C} - \left(\frac{2200}{T} \right) y_{Mn} \\ & + \left(\frac{3200}{T} + 2.1 \right) y_{Si} + \left(\frac{2000}{T} + 0.30 \right) y_{Ni} - \left(\frac{9500}{T} - 3.05 \right) y_{Cr} \\ & - \left(\frac{9500}{T} - 2.5 \right) y_{Mo} - \left(\frac{10700}{T} \right) y_{V} \end{aligned} \quad (9)$$

where y_i is the concentration parameter of element i , which can be expressed as $y_i = \frac{x_i}{1 - x_i}$, x_i is mole fraction of element i . Applying values in Table 1 into Eq. (9) gives the function of activity coefficient with absolute temperature. The value of η can be acquired from the work of Thomas [37] and is about 0.1676. Other parameters, for example E is chosen as 200 GPa, $\nu = 0.3$ and $1/\rho_0 = \frac{1}{4} \times (3.59726 \times 10^{-10})^3 \times 6.02 \times 10^{23} \text{ m}^3/\text{mol}$.

Using parameters and solve Eq. (8), the ratio of D_{app}/D_{zero} is plotted in Fig. 9. From the calculated results, it is obvious that the diffusion coefficient is increased by the diffusion-induced self-stress. The increasing level of carbon diffusion coefficient is up to two times at about 4.5 at.% of carbon contents. Comparing to the corresponding calculated values in Fig. 7 (more than five times), a gap between the diffusion coefficient still exists. Therefore the effect of self-stress on carbon diffusion only counts partially for the actual situation although it is rational that the carbon diffusion coefficients increase with carbon contents in respect of the elastic lattice expansion caused by carbon interstitials.

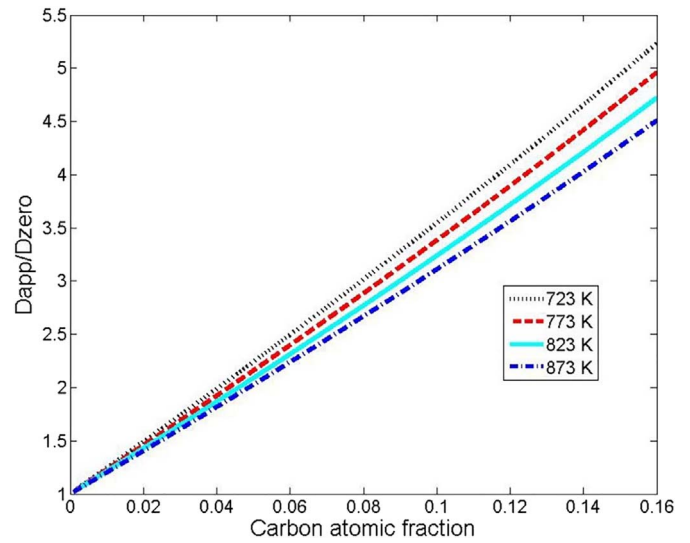


Fig. 9. Calculated curves of D_{app}/D_{zero} over carbon fraction at different temperatures.

4.3. Effect of external stresses and crystal orientation on interstitial diffusion

From experimental results as shown in Figs. 2, 3 and 4, it is apparent that the external compressive stresses applied on sample can suppress the diffusion of carbon in the carburized case. Considering the external stress effect on diffusion coefficient by applying an extra energy part $P \cdot \Delta V$, which influences the activation energy for carbon diffusion expressed in the following simple form:

$$D = D_0 \exp\left(-\frac{Q}{RT}\right) \cdot \exp\left(-\frac{P \cdot \Delta V}{RT}\right) \quad (10)$$

where P is the applied compressive stress and ΔV is the molar volume change of each carbon interstitials. Eq. (10) can be converted to a logarithmic form:

$$\ln D = \ln D_0 - \frac{Q + P \Delta V}{R} \left(\frac{1}{T} \right) \quad (11)$$

Therefore, from the slope of the plot $\ln D$ versus $1/T$, the activation energy is easily obtained. From the data obtained in Fig. 5, the calculated activation energy values with the change of carbon concentrations are shown in Fig. 10.

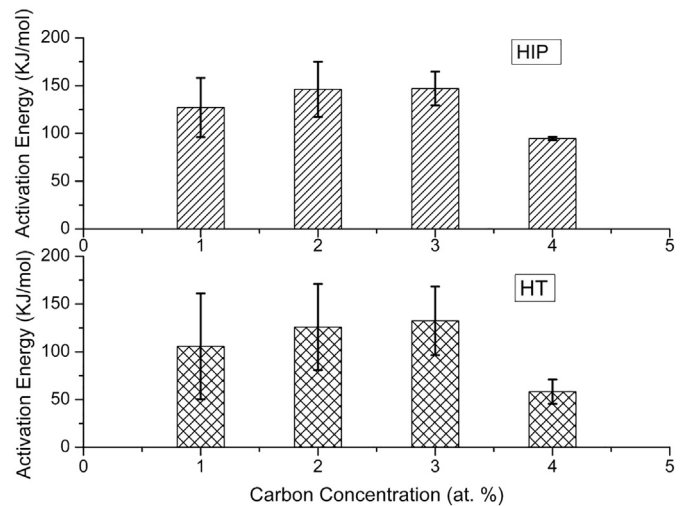


Fig. 10. Activation energy of carbon diffusion with the change of carbon concentrations (x axis are not continuous only represent 1 at.%, 2 at.%, 3 at.% and 4 at.%).

The activation energy is higher for HIPped sample (180 MPa iso-static compressive stress) than for HT sample. This is rational because the volume is expanded by carbon interstitials while the compressive stress suppressed such a volume expansion. It is worth noting that the activation energy dropped markedly at the higher carbon content (4 at. %) corresponding to an easier diffusion process at higher carbon contents. Meanwhile, the deviation of activation energy (nonlinearity) is larger at low carbon contents which probably suggested a variation of diffusion mode from higher carbon contents to lower one.

5. Conclusions

The effect of applied external compressive stress on carbon diffusion in supersaturated S-phase was studied in the research work by using HIP equipment and normal HT furnace on prior-carburized 316 austenitic stainless steel samples. Some conclusions can be made as follows:

1. The experimental results demonstrate that the compressive stress applied by HIP can retard the fast diffusion process comparing to the HT treated counterparts.
2. When heated at the same temperature, the activation energy of carbon diffusion is increased by applying an internal compressive stress via HIPping.

Acknowledgement

This research was sponsored by EPSRC, UK (EP/J018252/1) and NSFC, China (51201105) for the financial support. The authors express special thanks to Prof. Moataz Attallah in the Interdisciplinary Research Centre in Materials Processing of University of Birmingham for offering HIP equipment in this project.

References

- [1] H. Dong, S-phase surface engineering of Fe-Cr, Co-Cr and Ni-Cr alloys, *Int. Mater. Rev.* 55 (2010) 65–98.
- [2] F.A.P. Fernandes, T.L. Christiansen, G. Winther, M.A.J. Somers, On the determination of stress profiles in expanded austenite by grazing incidence X-ray diffraction and successive layer removal, *Acta Mater.* 94 (2015) 271–280.
- [3] B.K. Brink, K. Ståhl, T.L. Christiansen, C. Frandsen, M.F. Hansen, M.A.J. Somers, Composition-dependent variation of magnetic properties and interstitial ordering in homogeneous expanded austenite, *Acta Mater.* 106 (2016) 32–39.
- [4] B.K. Brink, K. Ståhl, T.L. Christiansen, J. Oddershede, G. Winther, M.A.J. Somers, On the elusive crystal structure of expanded austenite, *Scr. Mater.* 131 (2017) 59–62.
- [5] K. Marchev, R. Hidalgo, M. Landis, R. Vallerio, C.V. Cooper, B.C. Giessen, The metastable m phase layer on ion-nitrided austenitic stainless steels: part 2: crystal structure and observation of its two-directional orientational anisotropy, *Surf. Coat. Technol.* 112 (1999) 67–70.
- [6] N. Yasumaru, T. Bell, K. Akamatsu (Eds.), *Stainless Steel 2000: Thermochemical Surface Engineering of Stainless Steels* The Institute of Materials, London, 2000, pp. 229–245.
- [7] S. Thaiwattana, X.Y. Li, H. Dong, T. Bell, Comparison studies on properties of nitrogen and carbon S phase on low temperature plasma alloyed AISI 316 stainless steel, *Surf. Eng.* 18 (2002) 433–437.
- [8] Y. Cao, F. Ernst, G.M. Michal, Colossal carbon supersaturation in austenitic stainless steels carburized at low temperature, *Acta Mater.* 51 (2003) 4171–4181.
- [9] J. García Molleja, L. Nosei, J. Ferrón, E. Bemporad, J. Lesage, D. Chicot, J. Feugeas, Characterization of expanded austenite developed on AISI 316L stainless steel by plasma carburization, *Surf. Coat. Technol.* 204 (2010) 3750–3759.
- [10] C. Templier, J.C. Stinville, P. Villechaise, P.O. Renault, G. Abrasonis, J.P. Rivière, A. Martinavičius, M. Drouet, On lattice plane rotation and crystallographic structure of the expanded austenite in plasma nitrided AISI 316L steel, *Surf. Coat. Technol.* 204 (2010) 2551–2558.
- [11] J. García Molleja, M. Milanese, M. Piccoli, R. Moroso, J. Niedbalski, L. Nosei, J. Bürgi, E. Bemporad, J. Feugeas, Stability of expanded austenite, generated by ion carburizing and ion nitriding of AISI 316L SS, under high temperature and high energy pulsed ion beam irradiation, *Surf. Coat. Technol.* 218 (2013) 142–151.
- [12] J. Buhagiar, X. Li, H. Dong, Formation and microstructural characterisation of S-phase layers in Ni-free austenitic stainless steels by low-temperature plasma surface alloying, *Surf. Coat. Technol.* 204 (2009) 330–335.
- [13] Y. Sun, T. Bell, A numerical model of plasma nitriding of low alloy steels, *Mater. Sci. Eng., A* 224 (1997) 33–47.
- [14] S. Parascandola, W. Moller, D.L. Williamson, The nitrogen transport in austenitic stainless steel at moderate temperatures, *Appl. Phys. Lett.* 76 (2000) 2194–2196.
- [15] S. Mandl, B. Rauschenbach, Concentration dependent nitrogen diffusion coefficient in expanded austenite formed by ion implantation, *J. Appl. Phys.* 91 (2002) 9737–9742.
- [16] S. Mandl, F. Scholze, H. Neumann, B. Rauschenbach, Nitrogen diffusivity in expanded austenite, *Surf. Coat. Technol.* 174–175 (2003) 1191–1195.
- [17] G. Abrasonis, J.P. Rivière, C. Templier, L. Pranevičius, N.P. Barradas, Flux effect on the ion-beam nitriding of austenitic stainless-steel AISI 304L, *J. Appl. Phys.* 97 (2005) 124906.
- [18] T. Christiansen, K.V. Dahl, M.A.J. Somers, Simulation of nitrogen concentration depth profiles in low temperature nitrided stainless steel, *Defect Diffus. Forum* 258–260 (2006) 378–383.
- [19] T. Christiansen, K.V. Dahl, M.A.J. Somers, Nitrogen diffusion and nitrogen depth profiles in expanded austenite: experimental assessment, numerical simulation and role of stress, *Mater. Sci. Technol.* 24 (2008) 159–167.
- [20] D. Wu, Y. Ge, H. Kahn, F. Ernst, A.H. Heuer, Diffusion profiles after nitrocarburizing austenitic stainless steel, *Surf. Coat. Technol.* 279 (2015) 180–185.
- [21] T.L. Christiansen, M.A.J. Somers, Stress and composition of carbon stabilized expanded austenite on stainless steel, *Metall. Mater. Trans. A-Phys. Metall. Mater. Sci.* 40A (2009) 1791–1798.
- [22] J.C. Stinville, J. Cormier, C. Templier, P. Villechaise, Monotonic mechanical properties of plasma nitrided 316L polycrystalline austenitic stainless steel: mechanical behaviour of the nitrided layer and impact of nitriding residual stresses, *Mater. Sci. Eng. A* 605 (2014) 51–58.
- [23] W. Li, X. Li, Y.L. Chiu, H. Dong, On the thermo-mechanical stability and oxidation behavior of carbon S-phase at elevated temperature and under tensile stress, *Mater. Sci. Eng. A* 600 (2014) 90–98.
- [24] Y. SUN, X.Y. LI, T. BELL, X-ray diffraction characterisation of low temperature plasma nitrided austenitic stainless steels, *J. Mater. Sci.* 34 (1999) 4793–4802.
- [25] Y. Sun, X. Li, T. Bell, Structural characteristics of low temperature plasma carburized austenitic stainless steel, *Mater. Sci. Technol.* 15 (1999) 1171–1178.
- [26] W. Li, X. Li, H. Dong, Effect of tensile stress on the formation of S-phase during low-temperature plasma carburizing of 316L foil, *Acta Mater.* 59 (2011) 5765–5774.
- [27] J. Buhagiar, H. Dong, Low temperature plasma carbonitriding of ASTM F138 and ASTM F1586 biomedical stainless steels, *Surf. Eng.* 26 (2010) 256–264.
- [28] Y. Yang, M.F. Yan, Y.X. Zhang, C.S. Zhang, X.A. Wang, Self-lubricating and anti-corrosion amorphous carbon/Fe3C composite coating on M50NiL steel by low temperature plasma carburizing, *Surf. Coat. Technol.* 304 (2016) 142–149.
- [29] L. Boltzmann, Integration of diffusion equations by variable coefficients, *Ann. Phys.* 53 (1894) 959–964.
- [30] C. Matano, On the relation between the diffusion-coefficients and concentrations of solid metals (the nickel-copper system), *Jpn. J. Phys.* 8 (1933) 109–113.
- [31] F.C. Larche, J.W. Cahn, The effect of self-stress on diffusion in solids, *Acta Metall.* 30 (1982) 1835–1845.
- [32] F.C. Larche, J.W. Cahn, The interactions of composition and stress in crystalline solids, *Acta Metall.* 33 (1985).
- [33] F.C. Larche, J.W. Cahn, Phase changes in a thin plate with non-local self-stress effects, *Acta Metall. Mater.* 40 (1992).
- [34] J.W. Cahn, On spinodal decomposition, *Acta Metall.* 9 (1961) 795–801.
- [35] J.W. Cahn, On spinodal decomposition in cubic crystals, *Acta Metall.* 10 (1962) 179–183.
- [36] S.-J. Lee, D.K. Matlock, C.J. Van Tyne, Carbon diffusivity in multi-component austenite, *Scr. Mater.* 64 (2011) 805–808.
- [37] T.S. Hummelshøj, T.L. Christiansen, M.A.J. Somers, Lattice expansion of carbon-stabilized expanded austenite, *Scr. Mater.* 63 (2010) 761–763.